Biosensors and Bioelectronics 141 (2019) 111450

Contents lists available at ScienceDirect

Biosensors and Bioelectronics

journal homepage: www.elsevier.com/locate/bios

Hollow copper sulfide nanocubes as multifunctional nanozymes for colorimetric detection of dopamine and electrochemical detection of glucose

Junlun Zhu[a,1], Xu Peng[a,1], Wei Nie[a], Yijia Wang[a], Jingwen Gao[a], Wei Wen[a,**], Jonathan Nimal Selvaraj[b], Xiuhua Zhang[a], Shengfu Wang[a,*]

[a] Hubei Collaborative Innovation Center for Advanced Organic Chemical Materials, Ministry of Education Key Laboratory for the Synthesis and Application of Organic Functional Molecules, College of Chemistry and Chemical Engineering, Hubei University, Wuhan, 430062, PR China
[b] State Key Laboratory of Biocatalysis and Enzymrtic Engineering, College of Life Science, Hubei University, Wuhan, 430062, PR China

ARTICLE INFO

Keywords:
Nanozyme
Hollow copper sulfide nanocubes
Electrochemical sensing
Affinity
Colorimetric sensors

ABSTRACT

Nanozymes have fascinated increasing attention in the field of artificial enzyme. Designing an ideal nanozyme usually requires a synergic advantage of reasonable nanostructures and large specific surface area for ensuring excellent mimicking-enzyme catalytic activity. Here we report a CuS nanozyme with hollow nanocube structure (h-CuS NCs), which has a large surface area of 57.84 $m^2 g^{-1}$, and thus realizes excellent mimicking-enzyme catalytic activity. Expectedly, our directed design of h-CuS NCs nanozymes has an affinity for H_2O_2 of 0.94 mM, which is outstanding among the state-of-the-art Cu-based nanozymes. Furthermore, this nanozyme acts as a multifunctional catalyst to induce luminol chemiluminescence and oxide 3, 3′, 5, 5′-tetramethylbenzidine (TMB) in the presence of H_2O_2, and displays distinguished electrocatalytic activity to glucose oxidation. More intriguingly, the nanozyme can produce a promising photothermal effect under the illumination of near-infrared light. This work will provide a prototype for rational design of distinct nanostructures as multifunctional nanozymes in the area of electrochemical sensing, mimicking-enzyme catalytic biosening and cancer therapy.

1. Introduction

The directed evolution of enzymes, a directional selection of a mutant enzyme having the anticipated properties, has greatly satisfied growing advances in enzyme engineering technology and environmental and economic necessities for our daily life, of which artificial enzyme have emerged as high performance biocatalytic components for potentially fast and highly selective catalytic reactions (Benkovic and Hammes-Schiffer, 2013; Dydio et al., 2016; Wang et al., 2012). To subdue the limitations of natural enzymes, such as intrinsic instability, too narrow pH operational condition, and relatively high cost, directed evolution of enzymes have grown the most momentous means for improving critical traits of biocatalysts for a wide range of applications. Nowadays, the development of enzyme molecules is no longer in the status quo. Since the successfully preparation of fullerene derivatives in 1993 as a new member of artificial enzymes, the novel nanozymes have ignited a surge of unprecedented interests (Wang et al., 2016; Wei and Wang, 2013; Wu et al., 2018, 2019; Zhou et al., 2017). Nanozyme can work in harsh conditions (such as low durability, high temperature and extreme pH) compared to natural enzyme for biological and industrial applications. Generally, since commercially convenient enzyme-linked immunosorbent assay (ELISA) kits typically incorporate horseradish peroxidase as a label for the detection of numerous biomarkers, it is increasingly pay attention to develop nanozymes to mimic peroxidase activity (Gao et al., 2007). With careful design, the peroxidase activity of some nanomaterials exhibits many excellent biocatalytic activities and stability, which can be used to develop a wide variety of biosensors. For example, a large amount of nanomaterials, including noble metal nanomaterial (Lin et al., 2014; Zhao et al., 2016), carbon nanomaterials (carbon nanotubes, carbon dots, graphene quantum dots, etc.) (Du and Guo, 2016; Sun et al., 2018), transition metal oxide (Nasir et al., 2017; Xu and Qu, 2014), transitional metal dichalcogenides (Bai and Jiang, 2013; He et al., 2012; Shu et al., 2015; Yang et al., 2016), and metal organic frameworks (Chen et al., 2018; Cheng et al., 2017), have been developed with peroxidase-like activity thanks to their adjustable catalytic activity and affinity to the substrate. Although the fact that the catalytic activity of nanozymes offers convenience to disease diagnosis and antibacterial therapy, the directed design of nanozymes with

* Corresponding author.
** Corresponding author.
E-mail addresses: wenwei@hubu.edu.cn (W. Wen), wangsf@hubu.edu.cn (S. Wang).
[1] Those authors contributed equally to this work.

https://doi.org/10.1016/j.bios.2019.111450
Received 16 April 2019; Received in revised form 6 June 2019; Accepted 18 June 2019
Available online 20 June 2019
0956-5663/

specific structures to improve catalytic activity and application diversity is still under investigation.

Transitional metal dichalcogenides (TMDs), as an important member in the family of sulfur-containing nanomaterials, have fascinated largish attention in recent years due to their intriguing applications (Luo et al., 2019; Wang et al., 2017; Zhu et al., 2017). For instance, FeS_2 (Hu et al., 2015), SnS_2 (Jiao et al., 2017), Ni_3S_2 (Chen et al., 2017), Co_3S_4 (Zhao et al., 2014), MoS_2 (Gao et al., 2018; Li et al., 2018), CuS (Goel et al., 2014; Wang et al., 2018; Zeng et al., 2019), etc. have been widely used in batteries, supercapacitors, catalysis and sensing. On the other hand, Cu-based nanomaterials are similar to Fenton's reagent in solution and are known to catalyze the breakdown of hydrogen peroxide (H_2O_2). Therefore, Cu-based nanomaterials have good peroxidase mimetic performance with a wide range of applications in the field of nanozymes. The advantages of CuO, CuS, $Cu_3(PO_4)_2$, and Cu-based metal organic frameworks, etc. are widely used to simulate peroxidase, which is used to construct a sensing platform for detection of biomolecules (Huang et al., 2017; Zhu et al., 2018). In this regard, copper sulfide (CuS) nanostructures become a potential candidate for Cu-based nanozyme with good performance in the field of analytical science (Fan et al., 2016; Niu et al., 2018). In addition, hollow nanostructures have attracted great interest due to their interesting structurally induced physicochemical properties and the enormous potential for widespread application. Compared with solid counterparts, hollow nanostructures with permeable and porous shells, have many unique features including high surface area, low density, and high load carrying capacity(Lu et al., 2018; Yu et al., 2018a, 2018b). The hollow structures with high surface area can effective accommodate the strain during a chemical reaction and promoting complete penetration of the electrolyte(Fang et al., 2019). However, there is still plenty of room for improvement specific surface area for the rational design of distinct nanostructures for higher catalytic activity. Despite much progress, there have been few reports on the preparation of metal sulfides with complex hollow nanostructures and nanomaterials with peroxidase activity. Therefore, how to develop a novel nanostructured Cu-based nanomaterial with high surface area is still a challenge, but it will be of great significance for the design directed of an excellent nanozyme.

In this work, we have developed a hollow copper sulfide nanocubes nanozymes, realising excellent catalytic activity, better electrocatalytic and photothermal performance, good chemiluminescence and high affinity for H_2O_2 in the directed design of multifunctional nanozymes.(see Fig. 1) In our case, hollow CuS nanocubes (h-CuS NCs) are obtained by vulcanization at a suitable sodium sulfide concentration using a block of cuprous oxide as a template. h-CuS NCs not only offer the relatively large specific surface area due to the hollow nanostructure but also are similar to the characteristics of Fenton reagents, leading to better peroxidase-like performance. As expected, our directed design of h-CuS NCs nanozymes has better electrocatalytic performance for glucose at 0.5 V and has an affinity for H_2O_2 of 0.94 mM, which is outstanding among the state-of-the-art Cu-based nanozymes. Furthermore, the nanozyme can be used for electrocatalytic detection of glucose and can produce a promising photothermal effect under the illumination of near-infrared light. In addition, electrochemical detection of glucose exhibited good linearity from 0.1 mM to 10 mM and colorimetric detection of dopamine exhibited good linearity from 2 to 150 μM with a calculated detection limit (LOD = 3σ/S) of 1.67 μM. Therefore, the h-CuS NCs nanozymes suggests that the structure of hollow nanocubes could be used to some filed, such as drug delivery, cancer therapy, wastewater treatment, etc.

2. Materials and methods

2.1. Chemicals and materials

Polyvinyl pyrrolidone (PVP) (Mw = 10000), copper(II) chloride dehydrate ($CuCl_2$ $2H_2O$), sodium hydroxide (NaOH), dopamine hydrochloride, sodium hydrogen sulfide nonahydrate (Na_2S $9H_2O$), 3, 3′, 5, 5′-tetramethylbenzidine (TMB), hydrogen peroxide (H_2O_2), L-ascorbic acid, p-phthalic acid (PTA) horseradish peroxidase (HRP) and glacial acetic acid were purchased from Aladdin Reagent Co., Ltd (Shanghai, China). Nafion was obtained from Format New Energy Technology Co., Ltd (Shanghai, China). Ethanol and other reagents were purchased from Sinopharm Chemical Reagent Co., Ltd (Shanghai, China). All other reagents were analytical grade. The use of ultrapure water (18.25 MΩ cm) throughout the course of the experiment was from the Aquapro water purification system. Buffer solution was 0.1 M acetate buffer saline (pH 4.0) which was prepared with CH_3COOH (HAc) and CH_3COONa (NaAc). All solutions were prepared with ultrapure water.

2.2. Preparation of hollow copper sulfide nanocubes

Hollow copper sulfide nanocubes were synthesized by using cuprous oxide nanoparticles as a template (Yec and Zeng, 2012; Zhan and Zeng, 2016). In a typical experiment, firstly, 85.2 mg of $CuCl_2$ $2H_2O$ and 0.5 g of PVP were dissolved into 200 mL of water. After the solution was stirred for 5 min, 2.5 mL of 0.2 M NaOH was added dropwise. Then, 2.5 mL of 0.1 M L-ascorbic acid was dropwise added into the solution just 5 min after all NaOH was added. The mixture was continuously stirred for 5 min at room temperature. The solution was heated to 60 °C by heating in a water bath. Then, 2.0 mL of 1.0 M Na_2S aqueous solution was added to the above solution, and the solution immediately became black and reacted at 60 °C for 3 h under stirring. The unreacted impurity was washed out by three centrifugation steps with water and ethanol (12000 rpm for 8 min). The product was drying for future research.

2.3. The evaluation of catalytic activity

The enzyme mimetic peroxidase activity of hollow copper sulfide nanocubes was investigated through the catalytic oxidation of the peroxidase substrate TMB in the presence of H_2O_2. The kinetic data were obtained by changing H_2O_2 concentration as substrate while fixing of TMB concentration, or vice versa. All the reactions were incubated in 0.1 M acetate buffer saline (pH 4.0) and were measured in time scan mode at 652 nm by a UV-Vis spectrophotometer. Kinetic measurements were carried out in time course mode by monitoring the absorbance change of TMB at 652 nm. For the peroxidase-like catalytic

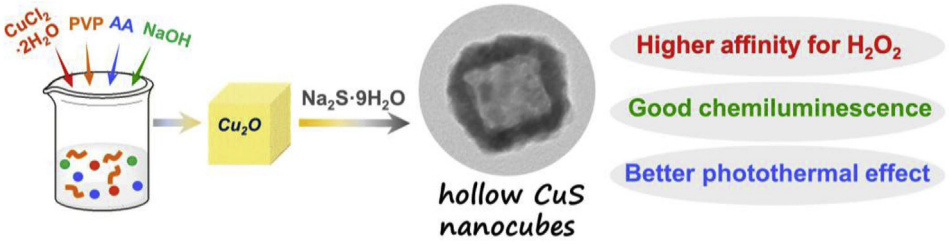

Fig. 1. Synthesis strategy for a hollow CuS nanocube with higher affinity for H_2O_2.

activity tests, to a reaction volume of 3 mL, 20 μL of 1 mg mL^{-1} h-CuS NCs, and different concentrations of TMB and H_2O_2 were added.

2.4. The investigation of catalytic reaction mechanism

To investigate the catalytic reaction mechanism, ·OH was evaluated by using p-phthalic acid (PTA) as a fluorescence probe in the h-CuS NCs–H_2O_2 system, which was widely used for the detection of ·OH. 20 μL of 1 mg mL^{-1} h-CuS NCs, 20 μL of 30% H_2O_2 and 1 mL of 2 mM PTA were mixed at room temperature in a total volume of 3 mL. The fluorescence intensity at different times was recorded using a RF-5301PC fluorescence spectrophotometer.

2.5. Detection of dopamine

Dopamine detection was conducted as follows: 2830 mL of 0.1 M acetate buffer saline (pH 4.0), 30 μL of 10 mM TMB, 20 μL of 30% H_2O_2 and 20 μL of 1 mg mL^{-1} h-CuS NCs and 100 μL of different concentration of dopamine were placed in a centrifuge tube. The total volume is kept at 3 mL. After shaking, the solution was incubated at room temperature for 30 min, and 100 μL of dopamine solutions of different concentrations were added. Then, the solutions were incubated for another 3 min. A UV-Vis spectrophotometer was used for analysis of the solutions in the 652 nm, and the corresponding absorption spectra were obtained.

2.6. Characterization

The morphology of the as-prepared and h-CuS NCs was studied using a FEI-Tecnai G2 F30 transmission electron microscope (TEM) operating at an acceleration voltage of 100 kV. Powder X-ray diffraction (XRD) were recorded on a Bruker D8A25 diffractometer with Cu Kα radiation (λ = 1.5418 Å) operating at 40 kV and 40 mA. Fluorescence spectra were measured on a RF-5301PC fluorescence spectrophotometer which was purchased from Shimadzu Ltd., (Japan). Ultraviolet-visible (UV-Vis) absorption spectra were performed on a UV-Vis spectrophotometer (UV-2700, Shimadzu, Japan). Fourier-transform infrared (FT-IR) spectra were collected on NICOLET iS10 spectrophotometer (Thermo scientific, USA) using KBr pellets technique in the range of 4000 cm^{-1} to 400 cm^{-1}. X-ray photoelectron spectroscopy (XPS) measurements were carried out on an ESCALAB 250Xi instrument. The Brunauer-Emmett-Teller (BET) method was utilized to calculate the specific surface areas were calculated by using the Barrett-Joyner-Halenda (BJH) method.

3. Results and discussion

3.1. Characterization of Cu-based nanomaterials

The h-CuS NCs were successfully prepared with peroxidase-like activity using the freshly prepared Cu_2O nanoparticles as a template by one pot method. A series of systematic characterization of h-CuS NCs is shown in Fig. 2. As illustrated in Fig. 2A, the X-ray diffraction (XRD) pattern of the synthesized h-CuS NCs and the standard diffraction peaks were presented. It is ascertained that all the peaks of the freshly prepared sample coincide with the hexagonal phase of the covellite structure (JCPDS-PDF 06–0464, a = b = 3.792 Å, c = 16.344 Å). The results showed the h-CuS NCs are favorable crystallinity and the high purity of CuS samples. Meanwhile, the XRD pattern of Cu_2O nanocubes as precursor of h-CuS NCs can be assigned perfectly to cubic cuprous oxide (JCPDS 05–0667, a = b = c = 4.2696 Å), confirming the pure phase of Cu_2O. The Cu_2O samples appeared cubical and homogeneous with an expected size of about 50 nm. (Fig. S1). To further scrutinized the morphology and crystallographic characteristics of the h-CuS NCs, the morphology and nanoparticles size of the as-prepared h-CuS NCs were obtained using transmission electron microscopy (TEM) and high resolution transmission electron microscopy (HRTEM). Fig. 2B showed a TEM image of the synthesized h-CuS NCs which showed hollow cube-like crystals uniformly dispersed with a size of 50 nm. The HRTEM image of the h-CuS NCs (Fig. 2C) revealed two distinct lattice fringes, where d = 0.305 nm is assigned to the (102), and d = 0.322 nm is assigned to the (101), which are well consistent with the XRD results of h-CuS NCs. In addition, to determine surface functional groups of as-synthesized h-CuS NCs, the FT-IR spectroscopy of the pure h-CuS NCs and polyvinyl pyrrolidone (PVP) were performed. As depicted in Fig. S2, the absorption bands at 2949, 1660, 1458, 1442, and 1294 cm^{-1} can be corresponded to the PVP molecules. This result means that h-CuS NCs may contain PVP molecules as a support. The peak at 3429 cm^{-1} is attributed to the stretching mode of the hydroxyls of adsorbed water. Curve black in Fig. S2 showed the FT-IR spectrum of h-CuS NCs, which exhibited the typical vibrational bands of C–S and Cu–S in the region of 1111 and 619 cm^{-1}, respectively (Nie et al., 2013). These absorption peaks reflect that CuS was effectively and successfully prepared by a one pot method.

Furthermore, XPS analysis of h-CuS NCs was conducted to further identify chemical environment. The survey spectrum of h-CuS NCs, as depicted in Fig. 2D, symptomatizes the presence of C, N, O, S and Cu element in h-CuS NCs samples. The XPS spectrum of C, N, and O are derived from the precursor PVP. Fig. 2E displays the XPS of S 2p with the peaks of 163.2 eV and 161.9 eV corresponded to the binding energies of S $2p_{1/2}$ and S $2p_{3/2}$, respectively, which are separated by a spin-orbit splitting of 1.3 eV that is also being coincident with the reported value (Cho et al., 2016). The high resolution XPS spectra of Cu 2p in Fig. 2F displayed two peaks at 932.5 eV and 952.4 eV, which ascribed to Cu $2p_{3/2}$ and Cu $2p_{1/2}$, respectively. The separation of two peaks is 19.9 eV, indicating a +2 oxidation state for the Cu ion (An et al., 2015; Cho et al., 2016; He et al., 2012). As shown in Fig. S3, it worth noting that the specific surface area as determined using the N_2 adsorption isotherm of h-CuS NCs was calculated to be 57.84 $m^2 g^{-1}$, which is obviously larger than that of general solid CuS 34.76 $m^2 g^{-1}$, showing promising signs for high catalytic activity. Compared to previous hollow copper sulfide (Shu et al., 2015), h-CuS NCs have a larger specific surface area resulting in better catalytic activity.

3.2. Peroxidase-like activity of h-CuS NCs

For estimating the catalytic activity of h-CuS NCs, the kinetic analysis of h-CuS NCs with peroxidase-like activity was further investigated using apparent steady state kinetic experiments for the oxidation of 3, 3′, 5, 5′-tetramethylbenzidine (TMB) in the presence of H_2O_2. As shown in Fig. 3, the kinetic data were obtained by using a range of different concentrations of TMB at a prescribed and excessive H_2O_2 concentration or a series of different concentrations of H_2O_2 at a prescribed and excessive TMB concentration. The catalytic properties apply to the typical Michaelis-Menten model. Michaelis-Menten kinetics equation

$$V = (V_{max}[S])/(K_m + [S])$$

$$1/V = (K_m/V_{max})(1/[S]) + 1/V_{max}$$

is accustomed to formulate the rate of enzymatic reactions. In the equation, where V represents the initial velocity, K_m represents the Michaelies-Menten constant, V_{max} represents the maximal reaction velocity and $[S]$ represents the concentration of the substrate. The K_m and V_{max} are received from the slope and intercept in the Lineweaver-Burk double reciprocal plot, which shows a good linear relationship between V^{-1} and $[S]^{-1}$. It is known that K_m and V_{max} are two key parameters for quantifying the catalytic ability of an enzyme, where K_m is the affinity of the enzyme to its substrate. The main manifestation is that the smaller the K_m value, the higher the affinity of the enzyme for the substrate. V_{max} describes the reactivity of the enzyme when it is saturated with the substrate. Therefore, K_m and V_{max} are one of the important reference standards for judging the superiority of the enzyme.

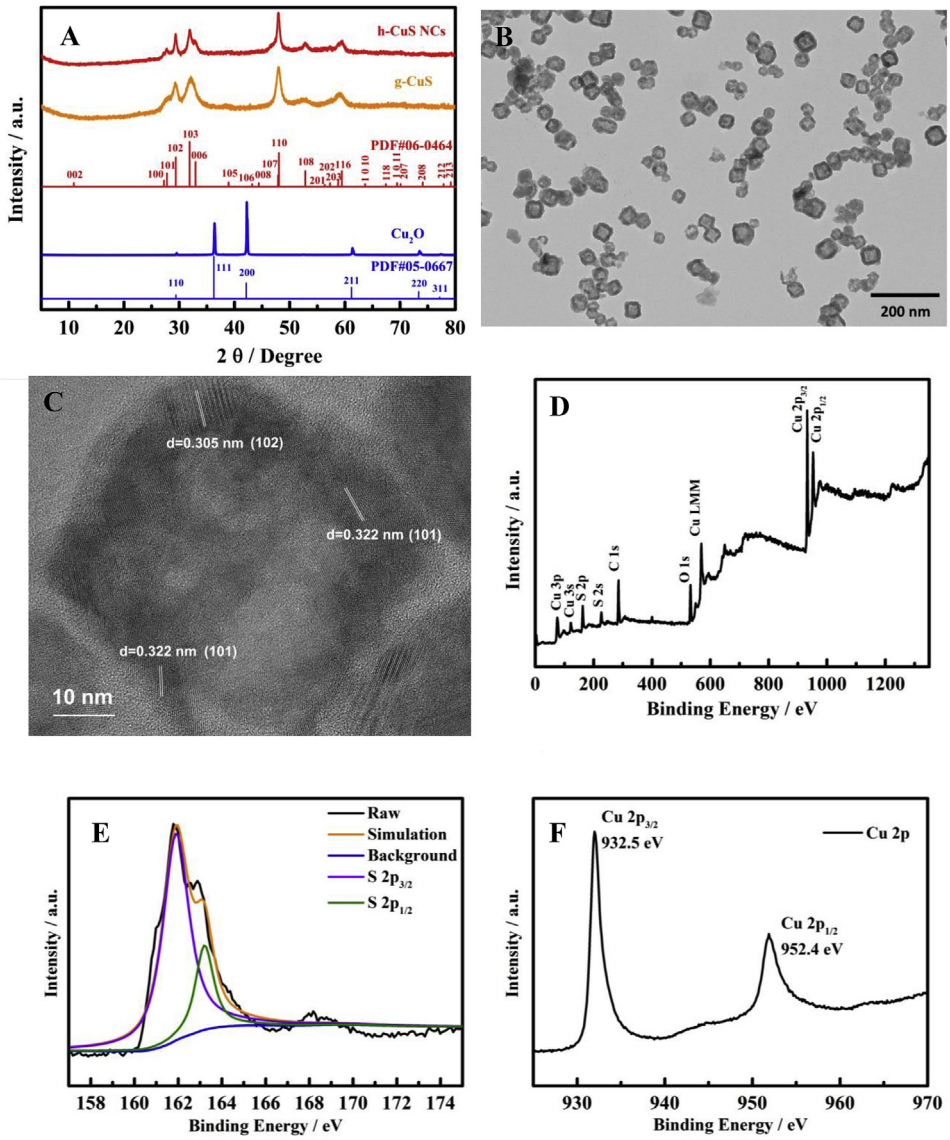

Fig. 2. (A) XRD patterns of h-CuS NCs and the standard CuS materials. (B) TEM image of h-CuS NCs. (C) HRTEM image of h-CuS NCs. XPS spectra of h-CuS NCs: (D) full survey spectrum, (E) S 2p, (F) Cu 2p.

The important enzyme parameters K_m and V_{max} values for h-CuS NCs and horseradish peroxidase (HRP) were listed in Table S1. In this work, the K_m value of h-CuS NCs with TMB as a substrate was displayed 1.62 mM, and when H_2O_2 as a substrate, the corresponding K_m value was displayed 0.94 mM. As shown in Fig. S4, the K_m value of HRP with TMB as a substrate was displayed 0.53 mM, and when H_2O_2 as a substrate, the corresponding K_m value was displayed 2.61 mM. It is praiseworthy mentioning that the K_m (H_2O_2) value of h-CuS NCs is much lower than that of other nanomaterials and HRP (3.7 mM) (Gao et al., 2007), indicating that h-CuS NCs have a relatively high binding affinity for H_2O_2. Therefore, it also shows that h-CuS NCs have good peroxidase-like catalytic activity.

3.3. Study on the electrocatalysis of h-CuS NCs

In order to investigate its electrocatalytic activity, we used electrocatalytic oxidation of glucose as a research object. The mechanism of glucose oxidation on CuS modified electrode in alkaline medium is similar to that of copper(Radhakrishnan et al., 2016). The oxidation peak of glucose is due to the initial oxidation of CuS to CuSOH and the process of maintaining high oxidation of Cu^{3+} in the center of Cu. The whole process can be clearly explained as follows: $CuS + OH^- \rightarrow CuSOH + e^-$. Then, the deprotonation of glucose in an alkaline line medium initiate isomerization to an enediol structure, which contact with Cu^{3+} gets oxidized into gluconolactone and then further hydrolyzes into gluconic acid(Ling et al., 2018; Qian et al., 2013; Radhakrishnan et al., 2016). The cyclic voltammetry was recorded to study the electrocatalytic behavior of glucose by modified electrode. Fig. 4A and B showed the CVs of the electrode in 0.1 M NaOH at a scanning rate of 50 mV s^{-1} in the absence (Fig. 4A) and presence (Fig. 4B) of 10 mM glucose. It could be seen that bare GCE, Nafion/GCE, and Nafion/CuS nanozymes/GCE displayed almost no electrochemical response in the absence of glucose. After adding 10 mM glucose, bare GCE, Nafion/GCE, and Nafion/CuS nanozymes/GCE still showed good electrochemical response. Therefore, the chronoamperometry (i-t) measurements were carried out. The current analysis of the h-CuS NCs/Nafion electrode was carried out at a constant potential of 0.50 V by injecting 20 μL of different concentrations of glucose into a 0.1 M NaOH solution while maintaining the total volume of the solution at 3.0 mL. As shown in Fig. 4C, all h-CuS NCs modified electrodes exhibited a sensitive current response to different concentrations of glucose, indicating that h-CuS NCs are an excellent electrocatalyst. During the

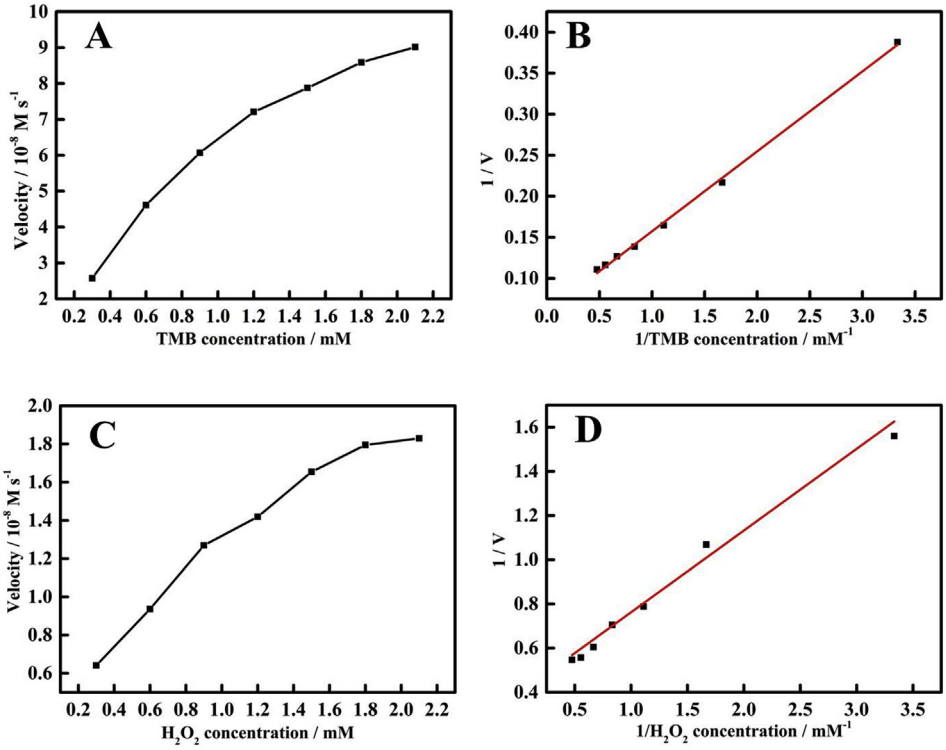

Fig. 3. Steady-state kinetic analysis of h-CuS NCs as peroxidase mimetics. The system reaction rate was measured using 20 μL of 1 mg mL^{-1} h-CuS NCs in 0.1 M NaAc-HAc buffer (pH = 4.0) containing various concentrations of H_2O_2 and TMB. (A) The H_2O_2 concentration was 30 mM and the concentration of TMB was varied. (C) The TMB concentration was 0.5 mM and the concentration of H_2O_2 was varied. (B and D) The Lineweaver-Burk double reciprocal plots of activity of h-CuS NCs with the concentration of one substrate (H_2O_2 or TMB) fixed and the other varied.

response of the current, as the glucose concentration increased, a significant increase in the oxidation current was observed. It is shown in the inset of Fig. 4A that the low concentration glucose solution also has a good current response. Since h-CuS NCs/Nafion has a non-enzymatic electrochemical response current for different concentrations of glucose, the calibration curves of oxidation current and different concentrations of glucose are described in Fig. 4D. The linear relationship is presented in a concentration range of glucose concentrations from 0.1 mM to 10 mM and the linear curve is I (μA) = 7.18 c (mM) + 0.73 (R^2 = 0.9976). These data demonstrate that h-CuS NCs show excellent sensitivity to electrocatalytic oxidation of glucose and can monitoring of glucose in samples.

3.4. Study on the catalytic mechanism of h-CuS NCs

In order to explore its possible peroxidase-like catalytic mechanism, we verified it by fluorescence method (Zhou et al., 2018). Briefly, the addition of p-phthalic acid (PTA) as ·OH capture agent to the reaction

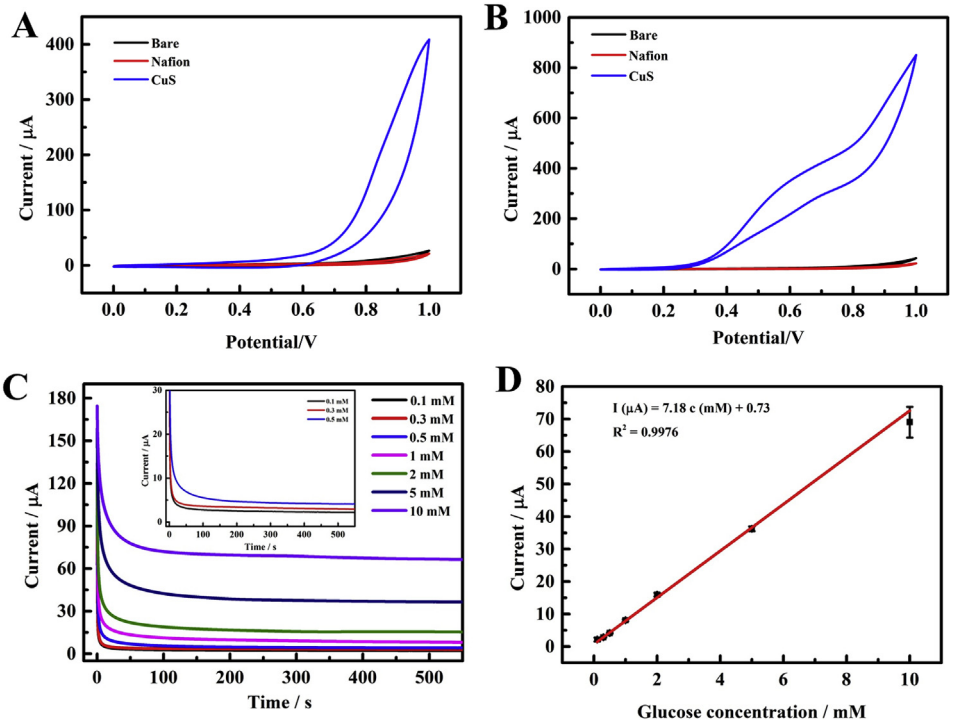

Fig. 4. (A) Cyclic voltammetry of bare GCE, Nafion/GCE, and Nafion/CuS nanozymes/GCE in 0.1 M NaOH in the absence of 10 mM glucose at a scan rate of 50 mV s^{-1}. (B) Cyclic voltammetry of bare GCE, Nafion/GCE, and Nafion/CuS nanozymes/GCE in 0.1 M NaOH in presence of 10 mM glucose at a scan rate of 50 mV s^{-1}. (C) Chronoamperometry responses of the h-CuS NCs/Nafion/GCE to different concentrations glucose of 0.1 mM, 0.3 mM, 0.5 mM, 1.0 mM, 2.0 mM, 5.0 mM, and 10.0 mM (from bottom to top). Insertion plot is 0.1 mM to 0.5 mM current response curve. (D) The calibration curve of current (μA) vs. the different concentration of glucose (mM). Error bars were taken from three parallel tests.

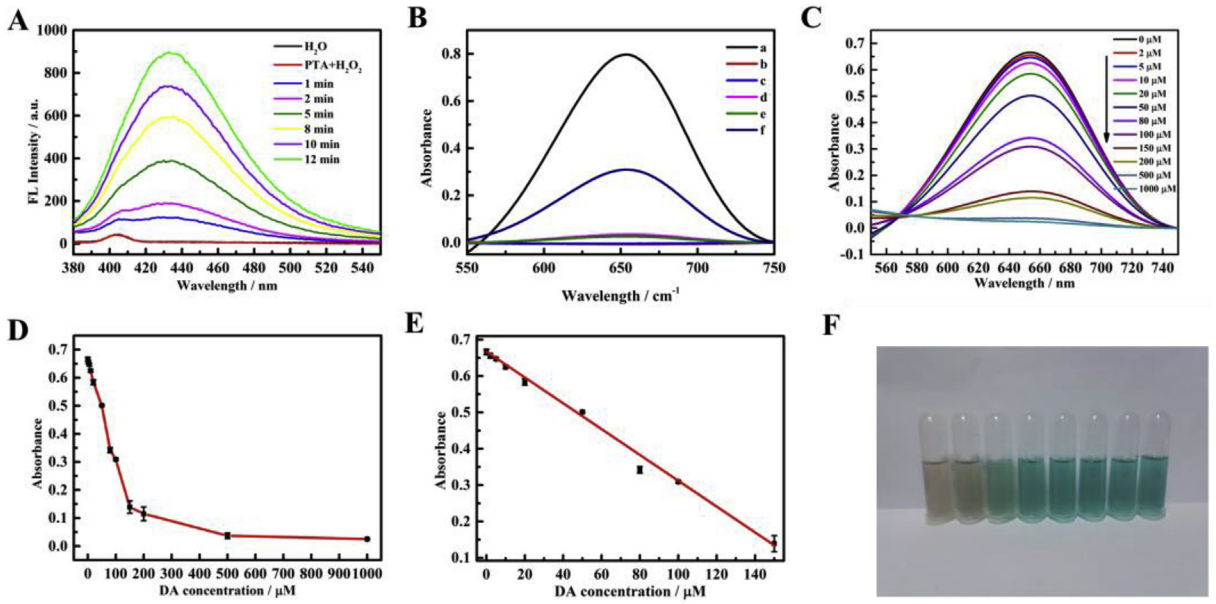

Fig. 5. (A) The fluorescence intensity of the H_2O_2 + h-CuS NCs system generated hydroxyl radicals captured by PTA changes with time. (B) The absorbance values at 652 nm in different reaction systems: (a) TMB + H_2O_2 + h-CuS NCs, (b) TMB + h-CuS NCs, (c) H_2O_2 + h-CuS NCs, (d) TMB + H_2O_2, (e) TMB + H_2O_2 + general CuS, (f) TMB + H_2O_2 + h-CuS NCs + 100 μM DA. (C) After reacting for 30 min with TMB (0.1 mM), H_2O_2 (0.2%), catalyst (20 μL 1 mg mL^{-1}) solution, 100 μL of different concentrations of DA were added to the mixed solution, and the UV-visible absorption curve was measured after 3 min. (D) The change in absorbance at 652 nm of the TMB mixed solution at different concentrations of DA. (E) A linear calibration curve of 2to 150 μL DA, the error bars represent for the standard deviation of three replicate measurements. Error bars were taken from three parallel tests. (F) The corresponding photographs of the color change of the mixed solution in the presence of 2to 150 μL DA, decrease from left to right, 150 μL, 100 μL, 80 μL, 50 μL, 20 μL, 10 μL, 5 μL, 2 μL. (For interpretation of the references to color in this figure legend, the reader is referred to the Web version of this article.)

system demonstrates the generation of hydroxyl radicals in the catalytic process of H_2O_2 catalyzed by h-CuS NCs. PTA itself is non-fluorescent, but it is very easy to couple with hydroxyl radicals to form highly fluorescent 2-hydroxyterephthalic acid, which emits unique blue fluorescence near 430 nm. As depicted in Fig. 5A, the fluorescence intensity showed an initial significant increase upon increasing time in the presence of PTA. These results confirmed that ·OH is derived from the decomposition of H_2O_2 by the catalysis of h-CuS NCs nanozyme and contributed to the oxidation of the PTA to form 2-hydroxyterephthalic acid with a blue fluorescent product. These results associated with h-CuS NCs suggest that h-CuS NCs act as peroxidases consistent with other materials.

3.5. Analytical application for determination of dopamine

To further investigate the peroxidase activity of h-CuS NCs, we investigated the UV/Vis spectra under different conditions. The UV/Vis absorption signal mainly obtains from the oxidation of TMB. Fig. 5B demonstrated the general pathway involved in the detection of dopamine (DA) using the h-CuS NCs-TMB-H_2O_2 system. DA, a main neurotransmitter, has various important roles in mammalians brain and body. DA is known to quench related reactive oxygen radicals and inhibit their oxidative capacity. Among these reactive oxygen groups, hydroxyl radicals are acknowledged to be one of highly active species which rapidly oxidize colorimetric substrates including TMB and O-phenylenediamine, during H_2O_2-mediated oxidation reactions. The reduction based on the DA amino group and the phenolic hydroxyl group could consume H_2O_2 by the redox reaction, and thus the oxidation of TMB by H_2O_2 was suppressed, and blue fading and a decrease in absorbance occurred at 652 nm. h-CuS NCs can catalyze the formation of H_2O_2 into ·OH, ·OH can oxidize colorless TMB to blue oxTMB, and ox-TMB can be reduced to TMB by DA(Dutta et al., 2015; Liu et al., 2018). Without DA, as shown in Fig. 5B, the absorbance of the mixture of TMB, H_2O_2, and h-CuS NCs was greatly enhanced. With DA, the absorbance of the mixture of TMB, H_2O_2, and h-CuS NCs was decreased. The h-CuS NCs has peroxidase-like activity which can catalyze the conversion of the colorless TMB to oxTMB with high absorbance peak at 652 nm. In a word, when a blue solution was present, blue fading or a decrease in absorbance may occur after the addition of DA. The reduced absorbance are directly proportional to the DA concentrations, therefore, the proposed method can be also applied to DA detection. To optimize the experimental conditions for DA sensing, some parameters (reaction time and response time) were explored by using h-CuS NCs-TMB-H_2O_2 system. A time-dependent absorbance was performed in Fig. S5, which shown that the absorbance increased with the time and descended in the range of 30to 40 min with the strongest absorbance at 30 min. Furthermore, we also explored the effects of DA response time. As shown in Fig. S6, the absorbance gradually decreased with the reaction time and get to the platform at 3to 4 min. Therefore, the optimal reaction time and response time were approximately 30 min and 3 min, respectively.

As a result, using this idea, a colorimetric method has also been applied in the detection of DA indirectly in this work. Fig. 5C showed the UV-vis absorption spectra recorded after the h-CuS NCs-TMB-H_2O_2 detection system in the presence of different concentrations of DA in NaAc-HAc solution (pH = 4.0) for 3 min. Obviously, the absorbance decreased with the increased concentration of DA. In addition, the color difference of the reaction system with different concentrations of DA is very obvious, and can even be recognized by the naked eye (Fig. 5F). Fig. 5D showed a typical DA concentration-absorbance change, which was obtained in the detection of DA. It has been observed that as the concentration of DA in the reaction mixture increases, it will indicate a decreased in the blue absorbance of the solution. The change in absorbance at a wavelength of 652 nm was monitored by introducing a DA solution under optimized conditions. The absorbance at 652 nm was plotted against the DA concentration in Fig. 5E, the linear regression equation was A = 0.6671–0.0036C (μM), where A marked the absorbance intensity at 652 nm and C marked the concentration of DA, and which shown a linear range of 2 to 150 μM with a calculated detection limit (LOD = 3σ/S) of 1.67 μM and a correlation coefficient R^2 = 0.9923. Additionally, the fabricated sensing system has good

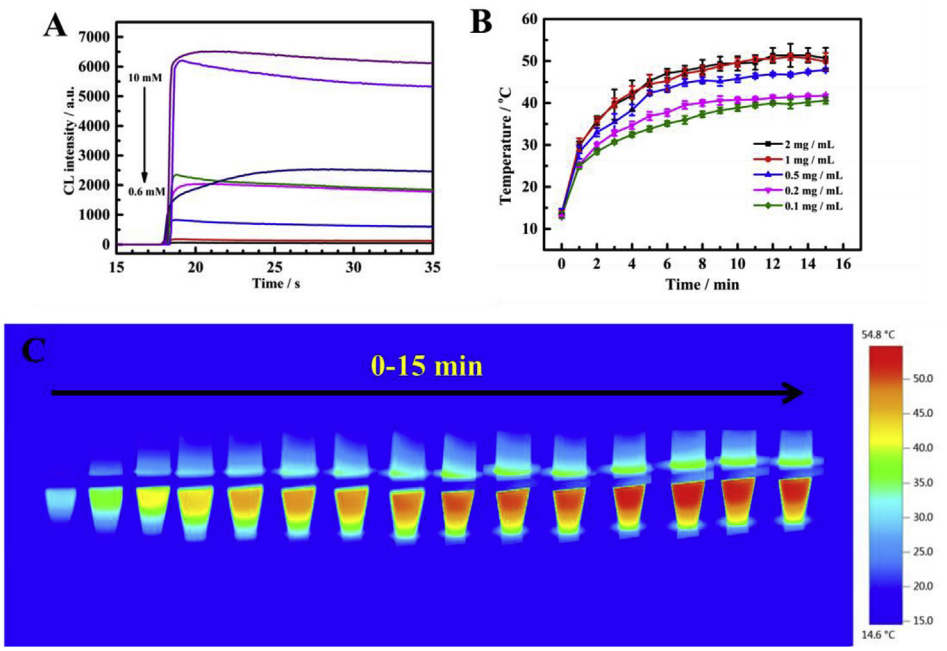

Fig. 6. (A) Chemiluminescence spectra measured to the oxidation of luminol by variable concentrations of H_2O_2 in MES buffer solution containing 0.2 mM luminol and 20 μL of 1 mg mL^{-1} h-CuS NCs. (B) Photothermal effect diagram of different concentrations of h-CuS NCs at 808 nm, where the error bars were obtained based on the thermal images. (C) thermal images of 2 mg mL^{-1} h-CuS NCs at different time ranging from 0 to 15 min.

reproducibility and selectivity for the detection of dopamine. As depicted in Fig. S8, 1.0 mM Urea, Glutamate, Glucose, Glucine, and Galactose have no obvious interference for the selective determination of 100 μM DA. To investigate the stability of the colorimetric detection platform, the absorbance was obtained by repeating 12 experiments (Fig. S7). The results indicated that the h-CuS NCs nanozyme can be used for colorimetric detection of dopamine with good stability in buffer solution.

3.6. Chemiluminescence and photothermal properties based on h-CuS NCs

Furthermore, in the presence of H_2O_2 and luminol, the h-CuS NCs catalyze the generation of chemiluminescence in the 2-morpholinoethanesulfonic acid (MES) buffer solution (pH = 6.0). This is mainly due to the fact that h-CuS NCs can generate a large amount of hydroxyl radicals for the chemiluminescence of luminol in the presence of H_2O_2. Fig. 6A represents the chemiluminescence spectra measured in the presence of 0.2 mM luminol and variable concentrations of H_2O_2. This experimental result indicated that h-CuS NCs can be used as a potential candidate for chemiluminescent signal labels. More importantly, we found that h-CuS NCs have a better photothermal effect. Fig. 6B shows that the temperature of the h-CuS NCs solution (2 mg mL^{-1}) reached 53.1 °C, the rate of temperature increase was 3.09 °C min^{-1}, and the temperature of ultrapure water was maintained at 28.3 °C the illumination of 808 nm at 15 min. Moreover, the temperature monotonically increased with increasing h-CuS NCs concentration and time, ranging from 0.1 to 2 mg mL^{-1} and 0–15 min, respectively (Fig. 6C). The h-CuS NCs produce significant local heat at 808 nm for a suitable period of time, and the high temperature environment effectively attenuates cancer cells. This indicated that h-CuS NCs will be able to be used as potential photothermotherapy agents and photodynamic therapeutics in biomedical and cancer treatments.

4. Conclusion

In conclusion, we have proposed a delicate templating strategy for the effective synthesis of novel hollow CuS nanocubes as heterogeneous catalysts to mimic peroxidase functions for the colorimetric detection of dopamine. The structure of h-CuS NCs exhibited an intermediate hollow cube and has a good specific surface area compared to general solid CuS. Additionally, we illustrated that the h-CuS NCs nanozyme can catalyze H_2O_2 to generate ·OH, which can oxidize TMB to produce a bule product (oxTMB) and dopamine can make it fade. Based on the strategy, a flexible colorimetric detection platform based on the h-CuS NCs nanozyme with peroxidase-like activity for dopamine detection was developed. The colorimetric detection of dopamine exhibited good linearity from 2 to 150 μM with a calculated detection limit (LOD = 3σ/S) of 1.67 μM. Furthermore, the prepared h-CuS NCs modified electrode was used to study the enzyme-free electrocatalytic glucose, and an electrochemical sensor was constructed for the detection of glucose. The electrochemical sensor detection of glucose exhibited good linearity from 0.1 mM to 10 mM. Finally, we used h-CuS NCs nanozyme as a research object to explore its chemiluminescence and photothermal properties. The experimental results revealed that the nanozyme can be used as a good chemiluminescent label and a better photothermal reagent with a heating rate of 3 °C min^{-1} on the illumination of 808 nm. This work may inspire further potentials for the design and construction of hierarchical hollow nanostructures with great complexity for diverse applications, such as drug delivery, cancer therapy, wastewater treatment, etc.

Declaration of interests

The authors declare that they have no known competing financial interests or personal relationships that could have appeared to influence the work reported in this paper.

CRediT authorship contribution statement

Junlun Zhu: Writing - original draft, Formal analysis. **Xu Peng:** Writing - original draft, Formal analysis. **Wei Nie:** Formal analysis. **Yijia Wang:** Formal analysis. **Jingwen Gao:** Formal analysis. **Wei Wen:** Funding acquisition, Investigation, Methodology, Project administration. **Jonathan Nimal Selvaraj:** Writing - review & editing. **Xiuhua Zhang:** Formal analysis. **Shengfu Wang:** Funding acquisition, Investigation, Methodology, Project administration.

Acknowledgements

This work was partly financially supported by the National Natural

Science Foundation of China (Nos.21405035, 21805074) and the General Project Program of the Natural Science Foundation of Hubei Province (No. 2017CFB529, 2018CFB151).

Appendix A. Supplementary data

Supplementary data to this article can be found online at https://doi.org/10.1016/j.bios.2019.111450.

Conflict of interest

The authors declare no conflict of interest.

References

An, L., Huang, L., Zhou, P.P., Yin, J., Liu, H.Y., Xi, P.X., 2015. Adv. Funct. Mater. 25, 6814–6822.
Bai, J., Jiang, X.E., 2013. Anal. Chem. 85 (17), 8095–8101.
Benkovic, S.J., Hammes-Schiffer, S., 2013. Science 301, 1196–1202.
Chen, P.Z., Zhou, T.P., Zhang, M.X., Tong, Y., Zhong, C.G., Zhang, N., Zhang, L.D., Wu, C.Z., Xie, Y., 2017. Adv. Mater. 29, 1701584.
Chen, W.H., Vázquez-González, M., Kozell, A., Cecconello, A., Willner, I., 2018. Small 14, 1703149.
Cheng, H.J., Liu, Y.F., Hu, Y.H., Ding, Y.B., Lin, S.C., Cao, W., Wang, Q., Wu, J.J.X., Muhammad, F., Zhao, X.Z., Zhao, D., Li, Z., Xing, H., Wei, H., 2017. Anal. Chem. 89, 11552–11559.
Cho, K., Han, S.H., Suh, M.P., 2016. Angew. Chem. Int. Ed. 128, 15527–15531.
Du, Y., Guo, S.J., 2016. Nanoscale 8, 2532–2543.
Dutta, S., Ray, C., Mallick, S., Sarkar, S., Sahoo, R., Negishi, Y., Pal, T., 2015. J. Phys. Chem. C 119, 23790–23800.
Dydio, P., Key, H.M., Nazarenko, A., Rha, J.Y.E., Seyedkazemi, V., Clark, D.S., Hartwig, J.F., 2016. Science 354, 102–106.
Fan, G.C., Zhu, H., Du, D., Zhang, J.R., Zhu, J.J., Lin, Y.H., 2016. Anal. Chem. 88, 3392–3399.
Fang, Y.J., Guan, B.Y., Luan, D.Y., Lou, X.W., 2019. Angew. Chem. 131, 7821–7825.
Gao, L.Z., Zhuang, J., Nie, L., Zhang, J.B., Zhang, Y., Gu, N., Wang, T.H., Feng, J., Yang, D.L., Perrett, S., Yan, X.Y., 2007. Nat. Nanotechnol. 2, 577–583.
Gao, Z.Q., Li, Y.Y., Zhang, X.B., Feng, J.H., Kong, L., Wang, P., Chen, Z.W., Dong, Y.H., Wei, Q., 2018. Biosens. Bioelectron. 102, 189–195.
Goel, S., Chen, F., Cai, W.B., 2014. Small 10, 631–645.
He, W.W., Jia, H.M., Li, X.X., Lei, Y., Li, J., Zhao, H.X., Mi, L.W., Zhang, L.Z., Zheng, Z., 2012. Nanoscale 4, 3501–3506.
Hu, Z., Zhu, Z.Q., Cheng, F.Y., Zhang, K., Wang, J.B., Chen, C.C., Chen, J., 2015. Energy Environ. Sci. 8, 1309–1316.
Huang, Y., Zhao, M.T., Han, S.K., Lai, Z.C., Yang, J., Tan, C.L., Ma, Q.L., Lu, Q.P., Chen, J.Z., Zhang, X., Zhang, Z.C., Li, B., Chen, B., Zong, Y., Zhang, H., 2017. Adv. Mater. 1700102.
Jiao, X.C., Li, X.D., Jin, X.Y., Sun, Y.F., Xu, J.Q., Liang, L., Ju, H.X., Zhu, J.F., Pan, Y., Yan, W.S., Lin, Y., Xie, Y., 2017. J. Am. Chem. Soc. 139, 18044–18051.
Li, F.Y., Li, Y.Y., Feng, J.H., Gao, Z.Q., Lv, H., Ren, X., Wei, Q., 2018. Biosens. Bioelectron. 100, 512–518.
Lin, Y.L., Ren, J.S., Qu, X.G., 2014. Adv. Mater. 26, 4200–4217.
Ling, P.H., Zhang, Q., Cao, T.T., Gao, F., 2018. Angew. Chem. Int. Ed. 57, 6819–6824.
Liu, J., Meng, L.J., Fei, Z.F., Dyson, P.J., Zhang, L., 2018. Biosens. Bioelectron. 121, 159–165.
Lu, Y., Yu, L., Wu, M., Wang, Y., Lou, X.W., 2018. Adv. Mater. 30, 1702875.
Luo, P., Zhuge, F.W., Zhang, Q.F., Chen, Y.Q., Lv, L., Huang, Y., Li, H.Q., Zhai, T.Y., 2019. Nanoscale Horiz. 4, 26–51.
Nasir, M., Nawaz, M.H., Latif, U., Yaqub, M., Hayat, A., Rahim, A., 2017. Microchim. Acta 184, 323–342.
Nie, G.D., Zhang, L., Lu, X.F., Bian, X.J., Sun, W.N., Wang, C., 2013. Dalton Trans. 42, 14006–14013.
Niu, X.H., Xu, X.C., Li, X., Pan, J.M., Qiu, F.X., Zhao, H.L., Lan, M.B., 2018. Chem. Commun. 54, 13443–13446.
Qian, L., Mao, J.F., Tian, X.Q., Yuan, H.Y., Xiao, D., 2013. Sensor. Actuator. B Chem. 176, 952–959.
Radhakrishnan, S., Kim, H.-Y., Kim, B.-S., 2016. Sensor. Actuator. B Chem. 233, 93–99.
Shu, Q.W., Li, C.M., Gao, P.F., Gao, M.X., Huang, C.Z., 2015. RSC Adv. 5, 17458–17465.
Sun, H.J., Zhou, Y., Ren, J.S., Qu, X.G., 2018. Angew. Chem. Int. Ed. 57, 9224–9237.
Wang, M., Si, T., Zhao, H.M., 2012. Bioresour. Technol. 115, 117–125.
Wang, X.Y., Hua, Y.H., Wei, H., 2016. Inorg. Chem. Front. 3, 41–60.
Wang, Y.H., Huang, K.J., Wu, X., 2017. Biosens. Bioelectron. 97, 305–316.
Wang, D.D., Dong, H.F., Li, M., Cao, Y., Yang, F., Zhang, K., Dai, W.H., Wang, C.T., Zhang, X.J., 2018. ACS Nano 12 (6), 5241–5252.
Wei, H., Wang, E.K., 2013. Chem. Soc. Rev. 42, 6060–6093.
Wu, J.J.X., Li, S.R., Wei, H., 2018. Chem. Commun. 54, 6520–6530.
Wu, J.J.X., Wang, X.Y., Wang, Q., Lou, Z.Q., Li, S.R., Zhu, Y.Y., Qin, L., Wei, H., 2019. Chem. Soc. Rev. 48, 1004–1076.
Xu, C., Qu, X.G., 2014. NPG Asia Mater. 6, e90.
Yang, Z.J., Cao, Y., Li, J., Lu, M.M., Jiang, Z.K., Hu, X.Y., 2016. ACS Appl. Mater. Interfaces 8 (19), 12031–12038.
Yec, C.C., Zeng, H.C., 2012. Chem. Mater. 24, 1917–1929.
Yu, L., Yu, X.Y., Lou, X.W., 2018a. Adv. Mater. 30, 1800939.
Yu, L., Yang, J.F., Guan, B.Y., Lu, Y., Lou, X.W., 2018b. Angew. Chem. Int. Ed. 57, 172–176.
Zhan, G.W., Zeng, H.C., 2016. Adv. Funct. Mater. 26, 3268–3281.
Zhao, W.W., Zhang, C., Geng, F.Y., Zhuo, S.F., Zhang, B., 2014. ACS Nano 8, 10909–10919.
Zhao, Y., Huang, Y.C., Zhu, H., Zhu, Q.Q., Xia, Y.S., 2016. J. Am. Chem. Soc. 138, 16645–16654.
Zeng, R.J., Zhang, L.J., Su, L.S., Luo, Z.B., Zhou, Q., Tang, D.P., 2019. Biosens. Bioelectron. 133, 100–106.
Zhou, Y.B., Liu, B.W., Yang, R.H., Liu, J.W., 2017. Bioconjug. Chem. 28, 2903–2909.
Zhou, L.L., Guan, Q., Li, Y.A., Zhou, Y., Xin, Y.B., Dong, Y.B., 2018. Inorg. Chem. 57, 3169–3176.
Zhu, C.Z., Du, D., Lin, Y.H., 2017. Biosens. Bioelectron. 89, 43–55.
Zhu, J.L., Nie, W., Wang, Q., Li, J.W., Li, H., Wen, W., Bao, T., Xiong, H.Y., Zhang, X.H., Wang, S.F., 2018. Carbon 129, 29–37.